# Signatures of molecular structure and dynamics in high–order harmonic generation

**Manfred Lein and Ciprian C. Chirilă**

**Institut für Physik, Universität Kassel**
**Heinrich–Plett–Straße 40, 34132 Kassel, Germany**

## 1 Introduction

High–order harmonic generation (HHG) [1, 2] is a phenomenon induced by intense laser fields. It refers to the conversion of a large number of laser photons into a single photon of high frequency. The generated frequencies are called high harmonics since they are — for sufficiently long incident laser pulses — integer multiples of the laser frequency. The generated radiation is coherent and therefore has properties similar to laser light: it emerges as a directed beam and can be temporally compressed into short pulses. The exact mechanism of the multiphoton process that produces harmonics depends on the target of laser irradiation. Harmonics from laser–plasma interaction have received much attention and bear great potential for the future [3], but these will not be discussed in this review. In the present–day applications, one works mostly with gas–phase harmonics, *i.e.* radiation emitted from atoms or molecules in a gas jet. Rare–gas atoms are the most frequently used target since they produce harmonics relatively efficiently. Nevertheless the intensity of the generated harmonics is generally small, namely about $10^{-5}$ or less of the incident laser light intensity. In typical experimental setups, laser pulses from Ti:Sapphire oscillators, *i.e.*, with wavelengths around 800 nm are used, and the harmonics range from the ultraviolet into the soft x-ray regime.

The gas–phase harmonics are — for high enough intensities — due to a three–step mechanism [4, 5]. In the first step, the system (atom or molecule) is ionized by the strong laser field; in the second step, the free electron is accelerated by the oscillating electric field of the laser pulse, and in the third step the electron returns to the positively charged core and can recombine under emission of a photon. The energy of this photon equals the kinetic energy of the returning electron plus the binding energy of the electron in the ground state of the system. For strong enough laser fields, the excursion length of the electron is much larger than the size of the atom, so that the motion of the continuum electron can be described classically in good approximation. The intuitive three–step model is based on the quasistatic picture of laser–atom interactions: changes of the time–dependent electric field are slow compared to the motion of bound electrons in the atomic ground state. This means that the ionization and recombination can be understood as nearly instantaneous events during which the value of the electric field is constant. The typical laser intensities are between $10^{14}$ and $10^{15}\,\mathrm{W/cm^2}$. The forces that the electric fields of such laser pulses exert on electrons are nearly as high as the forces between the nuclei and

the bound electrons. Therefore, the theoretical description must go beyond perturbation theory in the external field. On the other hand, the intensity is still below the regime where the magnetic field of the laser pulses or relativistic motion of the electrons start to play a role. It is therefore safe to employ the dipole approximation, where the magnetic field is neglected and the electron dynamics is described by the non-relativistic time–dependent Schrödinger equation (TDSE).

The recollision, the final step in the three–step model occurs on a time scale much faster than the optical period of the laser field, which is typically 2–3 fs. Therefore, recollisions give rise to attosecond bursts of harmonic radiation ($1\,\mathrm{as} = 10^{-18}\,\mathrm{s}$.) The generation of attosecond pulses has been one of the main areas of research within laser–matter interactions in recent years [6–12]. The current record in the production of the shortest isolated attosecond pulses is at 130 attoseconds pulse length [13]. With these extremely short pulses it is becoming possible to experimentally observe electronic motion in time, similarly to the observation of chemical reactions with femtosecond pulses. In femtochemistry [14], the pump–probe scheme is the standard method to observe dynamics: a femtosecond pump pulse starts a time–dependent process, and a femtosecond probe pulse is applied after a delay time to probe the state of the system. Since attosecond pulses are not strong enough yet to allow for attosecond–pump attosecond–probe schemes, one resorts to cross–correlation techniques where an attosecond pulse serves as the pump pulse and an infrared laser pulse probes the time evolution.

Besides using HHG as a light source for further applications, the last years have revealed that harmonics can also be exploited to obtain information about molecular properties [15–18]. Since the recombination step must lead back into the initial state of the molecule in order to give rise to coherent emission, the recombination probability depends strongly on the initial–state electronic wave function. Hence, HHG is very sensitive to the structure of the molecule. Furthermore, it is affected by any deviations of the molecular geometry from the initial geometry caused by the motion of the nuclei in the time between ionization and recombination. We will show in this review how these effects can be used towards the measurement of molecular structure and dynamics. Increasing efforts are presently made to pursue HHG from molecules. In particular, HHG with ensembles of laser–aligned molecules [19, 20] plays a central role. For example, alignment techniques opened the possibility to image molecular structure using the molecular–orbital tomography proposed by Itatani *et*

*al.* [16], which has attracted a tremendous amount of interest. The promise of such schemes is that they combine structure determination with the ultrahigh time resolution offered by femtosecond pulses. Even measurements with sub–femtosecond resolution have been achieved by exploiting the sub–laser–cycle duration of the recollision process [18]: electron wave packets can serve as an attosecond probe and therefore provide an alternative approach to attosecond physics, without the need for attosecond light pulses. This idea was used not only in HHG but also in the earlier work on recollision–induced molecular fragmentation [21, 22] where one measures fragment kinetic energies rather than harmonics.

The challenge for theoretical physics is twofold. On one hand, ab initio calculations are needed that aim for quantitative agreement with experiment. On the other hand, approximate models are equally important since they give more insight into the mechanisms of HHG, and since they provide the basis for schemes of molecular imaging using HHG. The theory of HHG consists of two building blocks: (i) the single–atom/single–molecule response to the laser field and (ii) the propagation of the laser field and the harmonics through the generating medium. We will concentrate on the first part only since we are interested in the signature of molecular properties in HHG.

The purpose of this article is to give a basic and easily accessible introduction into the theory of molecular HHG and to review the current developments in this field. In the following we will use atomic units, *i.e.* $m_\mathrm{e} = 1$, $\mathrm{e} = 1$, $\hbar = 1$, $4\pi\epsilon_0 = 1$ where $m_\mathrm{e}$ is the electron mass and e is the elementary charge. This means that the charge of the electron is $q_\mathrm{e} = -\mathrm{e} = -1$.

## 2 Theory of high–order harmonic generation

### 2.1 *Basic theory*

As explained in the introduction, the solution of the time–dependent Schrödinger equation is required to describe theoretically the interaction between molecules and the strong light fields of interest here. The Hamiltonian $H$ consists of the unperturbed part $H_0$ and the laser–molecule interaction $H_\mathrm{int}$. In the dipole approximation, the electric field $\mathbf{E}(t)$ of the laser pulse couples to the dipole operator $\mathbf{D}$ of the system so that the interaction is $H_\mathrm{int} = -\mathbf{D}\cdot\mathbf{E}(t)$. For fixed nuclei, the dipole operator depends on all the electron coordinates $\mathbf{r}_j$, namely $\mathbf{D} = -\sum_j \mathbf{r}_j$. We begin the discussion of the theory with the single–active–electron (SAE) approximation,

where we treat only one of the electrons as interacting with the laser field, while all other electrons remain "frozen", *i.e.*, they merely give rise to an effective, time–independent potential for the active electron. We then have $H_0 = \mathbf{p}^2/2 + V(\mathbf{r})$ and $H_{\rm int} = \mathbf{r} \cdot \mathbf{E}(t)$ with $\mathbf{r}$ being the coordinate of the active electron and $V$ the effective potential. The Hamiltonian in the form

$$H(t) = \frac{\mathbf{p}^2}{2} + V(\mathbf{r}) + \mathbf{r} \cdot \mathbf{E}(t) \tag{1}$$

is commonly known as the *length–gauge* Hamiltonian because the laser field couples to the "length" $\mathbf{r}$. An alternative treatment is the *velocity gauge*, where the Hamiltonian has the form

$$H(t) = \frac{(\mathbf{p} + \mathbf{A}(t))^2}{2} + V(\mathbf{r}) \tag{2}$$

with $\mathbf{A}(t) = -\int_{-\infty}^{t} \mathbf{E}(t')\, dt'$. Here, the laser–molecule interaction $H_{\rm int} = \mathbf{p} \cdot \mathbf{A}(t) + A(t)^2/2$ is governed by the canonical momentum $\mathbf{p}$, which, for a free electron, can be interpreted as a drift velocity. A third possibility is the treatment in the *acceleration gauge* or *Kramers–Henneberger frame* [23–27], which is the formulation in the accelerated reference frame of a free electron driven by the laser field. We will not discuss this approach in detail here. Observables have the same value independent of the chosen gauge as long as the TDSE is solved exactly. As soon as approximations are made, different gauges lead to different results. This happens for example if the calculation is carried out on a too small numerical grid or if one applies approximate schemes such as the strong–field approximation (SFA) that is described later in this review.

If the TDSE can be solved, we have the wave function $\Psi(t)$ at all times, and the next task is the calculation of the HHG spectrum. In classical electrodynamics, the spectrum of the dipole radiation emitted from a time–varying charge distribution is the power spectrum of the dipole acceleration, *i.e.*,

$$S(\omega) \sim |\mathbf{a}(\omega)|^2 \tag{3}$$

where $\mathbf{a}(\omega) = \int dt\, \mathbf{a}(t) \exp(\mathrm{i}\omega t)$ is the Fourier transform of the dipole acceleration $\mathbf{a}(t)$. In quantum mechanics, the same equation holds if the time–dependent expectation value of the dipole acceleration is used in place of $\mathbf{a}(t)$, *i.e.*, $\mathbf{a}(t) = \langle \hat{\mathbf{a}}(t) \rangle$ [28–31]. The dipole acceleration operator for one electron is $\hat{\mathbf{a}}(t) = \nabla V + \mathbf{E}(t)$. In the last equation, we have taken into account that the electron has negative charge.

The resulting spectrum then contains only the coherent part of radiation, *i.e.*, no spontaneous decay of excited states is included. One may ask

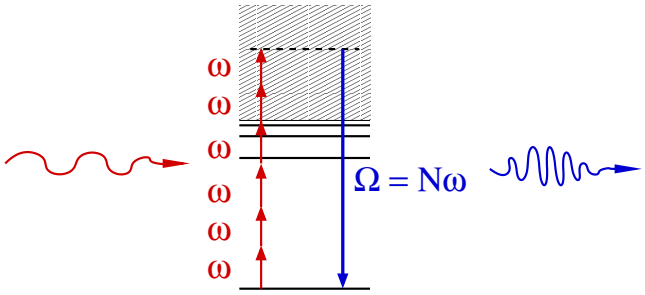


Fig. 1 Illustration of high–order harmonic generation as absorption and emission of photons.

what is the appropriate time interval over which the Fourier transformation of the acceleration should be evaluated. In principle, the integration runs over all times. But this is both impossible to do in a numerical calculation and also it would cause problems because an excited state will never decay to the ground state after the laser field has been turned off and therefore oscillations of the acceleration will continue indefinitely. (This is a shortcoming of the TDSE which treats the electromagnetic field classically.) Hence, in a practical calculation one normally works with laser pulses of finite duration $T_{\rm p}$ and the Fourier transform is taken only over the duration $T_{\rm p}$,

$$\mathbf{a}(\omega) = \int_0^{T_{\rm p}} dt\, \mathbf{a}(t) \exp(\mathrm{i}\omega t). \tag{4}$$

Nevertheless, one may sometimes choose a somewhat longer integration interval in order to obtain a more accurate harmonic spectrum. Notice that alternatively the spectrum can be calculated by first evaluating the time–dependent dipole moment and then taking the double derivative to obtain the dipole acceleration. This choice plays an important role in the context on the strong–field approximation, see Section 2.3. However, when harmonic spectra are calculated from the numerical solution of the TDSE, the method of choice is to evaluate the time–dependent dipole acceleration $\mathbf{a}(t)$ directly as the expectation value of the acceleration operator. It is less sensitive than the dipole moment to electron density far away from the nucleus and is thus less affected by the use of absorbing boundary conditions. Therefore the acceleration form usually produces a lower background noise level in the HHG spectra.

In the photon picture, HHG is understood as the absorption of a large number of photons from the incident laser field followed by emission of the absorbed energy in the form of one high–frequency photon, see Fig. 1. If the laser pulse has a small bandwidth, *i.e.*, the laser photon frequency has a sharp value, the harmonic emission spectrum will exhibit discrete frequencies, which are approximately integer multiples of the laser frequency.

### 2.2 *Three–step model*

A physical picture that is extremely useful to understand HHG is the semiclassical three–step model [4, 5]. It rests on the assumption that the laser–molecule interaction is approximately quasistatic, *i.e.*, it is meaningful to describe the interaction in terms of an instantaneous electric field. At time $t$ during the action of a laser pulse, the field–free binding potential $V_0$ for the active electron is distorted by the presence of the instantaneous electric field $\mathbf{E}(t)$. The total potential is

$$V(\mathbf{r}) = V_0(\mathbf{r}) + \mathbf{E}(t) \cdot \mathbf{r}. \tag{5}$$

In the quasistatic picture, the change of the electric field is slow compared to the bound–state electronic motion so that the electron wave function adjusts to the modified potential and the electron has time to tunnel through the potential barrier into the exterior region. The tunneling ionization process is shown schematically in Fig. 1. After ionization at a time $t_0$ (*first step*), the electron is strongly accelerated by the laser field with little influence from the binding potential. The electron dynamics can then be described classically in a good approximation. Since the electric field of a laser pulse oscillates, the electron will follow an oscillatory motion (*second step*). If the electron starts with zero velocity and the laser field is linearly polarized, the classical trajectory will be along a straight line, namely the laser polarization axis. For a monochromatic field polarized along the $z$-axis with electric field strength $E(t) = E_0 \sin(\omega t)$, one can immediately solve Newton's equation of motion, and one finds that the electron velocity $\dot{z}(t)$ is the sum of a sinusoidally oscillating term and a drift velocity,

$$\dot{z}(t) = \alpha\omega \cos(\omega t) - \alpha\omega \cos(\omega t_0). \tag{6}$$

Here,

$$\alpha = \frac{E_0}{\omega^2} \tag{7}$$

is the classical oscillation amplitude. The oscillation gives rise to a higher mean kinetic energy than from the drift velocity $v_{\mathrm{D}} = -\alpha\omega \cos(\omega t_0)$ alone.

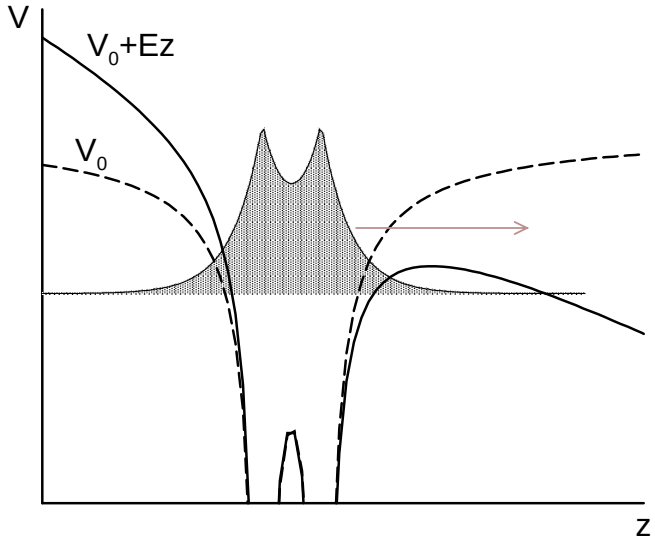


Fig. 2 Tunneling ionization in a diatomic molecule under the influence of an instantaneous electric field $E$ directed along the negative $z$-axis.

This additional kinetic energy due to the presence of the laser field is known as the ponderomotive potential

$$U_{\rm p} = \frac{E_0^2}{4\omega^2}. \tag{8}$$

If the electron starts at a suitable phase of the laser field, the trajectory can lead back to the core so that an electron–ion collision takes place (*third step*). With a small probability, the recollision causes recombination under emission of a photon — the high–harmonic photon. For a given starting time $t_0$, there may be zero, one or more solutions for the return time $t_1$. We refer to the difference $\tau = t_1 - t_0$ as the travel time or excursion time of the electron. For a monochromatic, *i.e.* purely sinusoidal time–dependence of the laser field, the kinetic electron energy at the time of return, $E_{\rm r}$, can be shown to have the maximum value $E_{\rm r,max} \approx 3.17\,U_{\rm p}$ [5]. In HHG, the emitted photon energy equals return energy plus binding energy of the electron in the ground state. This means that the cutoff in the HHG spectrum is at the photon energy $3.17\,U_{\rm p} + I_{\rm p}$, where $I_{\rm p}$ is the ionization potential of the molecule. Quantum mechanical corrections lead to the slightly modified cutoff $3.17\,U_{\rm p} + 1.32\,I_{\rm p}$ [32].

A given return energy can be realized by not only one but at least two different electron trajectories, known as the short and long trajectories.

Most HHG experiments are set up such that — taking advantage of the phase matching conditions for the generation of harmonics in a focused beam — only the short trajectories contribute significantly to the HHG spectrum [33–35]. For these short trajectories, one can fit the relation between the return energy and the travel time obtained from the classical model as

$$\omega\tau = 0.786[f(E_\mathrm{r}/U_\mathrm{p})]^{1.207} + 3.304[f(E_\mathrm{r}/U_\mathrm{p})]^{0.492}, \tag{9}$$

where $f(x) = \arccos(1 - x/1.5866)/\pi$. The fact that different return energies correspond to different return times $t_1$ makes the harmonic frequency dependent upon the emission time, *i.e.*, the harmonic radiation is *chirped* on a sub–femtosecond time scale [7].

From the three–step model it is apparent that harmonics are usually strongly suppressed when elliptical or circular laser polarization is used, because electrons starting with zero velocity do not return to the parent ion. We will see below, however, that an anomalous ellipticity dependence of harmonics may result from the initial electron momentum distribution.

### 2.3 *The strong–field approximation*

In order to arrive at a model that is capable of quantitatively predicting HHG spectra, we formulate the quantum mechanical version of the three–step model, which is known as the Lewenstein model or the strong–field approximation [32]. In the most widely used version of this theory, one first derives an expression for the time–dependent dipole moment $\mathbf{D}(t)$ due to the response of a single atom/molecule. Its dipole acceleration is then obtained as

$$\mathbf{a}(t) = \ddot{\mathbf{D}}(t), \tag{10}$$

and the HHG spectrum is calculated as described in Section 2.1. We restrict ourselves to the single–molecule response and do not investigate propagation effects. Furthermore, we begin with the length–gauge formulation based on the Hamiltonian (1) and with the assumption of fixed nuclei. In the strong–field approximation, one assumes that (i) the electron is unaffected by the laser field until the time $t'$ of ionization and (ii) afterwards the electron moves in the laser field only, unaffected by the binding potential. We also neglect the depletion of the bound state (which could be taken into account in principle). For a linearly polarized laser pulse with arbitrary electric field $E(t)$ such that $E(t < 0) = 0$, this leads to the dipole moment

(without terms corresponding to continuum–continuum transitions) [32]

$$\mathbf{D}(t) = -\mathrm{i}\int_0^t \mathrm{d}t' \int \mathrm{d}^3p\; \mathbf{d}_\mathrm{r}^*\big(\mathbf{p}+\mathbf{A}(t)\big)\, d_\mathrm{i}\big(\mathbf{p}+\mathbf{A}(t'),t'\big) \times \exp\big(-\mathrm{i}S(\mathbf{p},t',t)\big) \quad + \quad \text{c.c.} \tag{11}$$

where $S(\mathbf{p},t',t) = \int_{t'}^t \mathrm{d}t''[(\mathbf{p}+\mathbf{A}(t''))^2/2 + I_\mathrm{p}]$ is the semiclassical action, $I_\mathrm{p}$ is the ionization potential, $\mathbf{A}(t) = -\int_{-\infty}^t \mathbf{E}(t')dt'$, and the ionization and recombination matrix elements are given by

$$d_\mathrm{i}(\mathbf{p},t) = \langle\psi_\mathrm{PW}(\mathbf{p})|E(t)z|\psi_0\rangle, \tag{12}$$

$$\mathbf{d}_\mathrm{r}(\mathbf{p}) = \langle\psi_\mathrm{PW}(\mathbf{p})|-\mathbf{r}|\psi_0\rangle. \tag{13}$$

Here, $\psi_0$ is the field–free ground state, and $\psi_\mathrm{PW}(\mathbf{p})$ denote plane–wave states with momentum $\mathbf{p}$, normalized in the momentum scale, *i.e.*, $\langle\psi_\mathrm{PW}(\mathbf{p})|\psi_\mathrm{PW}(\mathbf{p}')\rangle = \delta(\mathbf{p}-\mathbf{p}')$. The appearance of plane waves is the essential point of the SFA. It facilitates partially analytical computation, but is the main source of errors at the same time.

The SFA expression (11) for the electronic dipole moment can be obtained in different ways: One way is to follow the original approach of [32], where an ansatz is made for the wave function. This ansatz, together with the aforementioned assumptions about the physical process lead to the results of Eq. (11). Another way, more straightforward, is based on the Dyson equation for the evolution operator:

$$\hat{U}(t,t') = \hat{U}_0(t,t') - i\int_{t'}^t dt''\,\hat{U}(t,t'')E(t'')z\hat{U}_0(t'',t'), \tag{14}$$

where $\hat{U}_0$ stands for the evolution operator associated with the field–free Hamiltonian. This is an integral equation, whose solution can be approximated by replacing in the right–hand side the full evolution operator $\hat{U}$ by the Volkov propagator $\hat{U}_\mathrm{V}$. The latter describes the evolution of an unbound electron under the influence of the electric field of the laser only. The replacement assumes that the main influence on the electron dynamics comes from the laser field and less from the binding Coulomb potential, which does not play any role between the ionization time $t''$ and the recombination time $t$ in (14). As a consequence, the low–energy part of the harmonic spectrum is poorly represented. One reason is that in this energy interval the bound–bound dynamics plays a significant role. As a general remark, low energy electrons (responsible for the emission of low–energy harmonics) 'feel' more than high–energy electrons the influence of the binding potential. For this reason, the SFA does not reproduce satisfactorily

the above–threshold ionization spectrum close to zero kinetic energy of the emitted electron, but it describes well the high–energy electrons.

With this in mind, the SFA expression for the evolution operator reads

$$\hat{U}^{\mathrm{SFA}}(t,t') = \hat{U}_0(t,t') - i\int_{t'}^{t} dt''\, \hat{U}_{\mathrm{V}}(t,t'')E(t'')z\hat{U}_0(t'',t'). \qquad (15)$$

Once the evolution operator is approximated as in Eq. (15), the electronic dipole moment can be easily calculated by inserting the approximated wave function $\psi(t) = \hat{U}^{\mathrm{SFA}}(t,0)\psi_0$ in the expression for the electron dipole moment $\mathbf{D}(t) = \langle\psi(t)| - \mathbf{r}|\psi(t)\rangle$. The continuum–continuum transitions [*i.e.*, the terms containing two integral terms from the right–hand side of Eq. (15)] are ignored, since they do not contribute significantly to the harmonic spectrum. One intermediate step to obtaining the result (11) is to replace the Volkov propagator by its spectral decomposition:

$$\hat{U}_{\mathrm{V}}(t,t') = \int d^3p\, |\psi_{\mathrm{V}}(\mathbf{p},t)\rangle\langle\psi_{\mathrm{V}}(\mathbf{p},t')|, \qquad (16)$$

with $\psi_{\mathrm{V}}(\mathbf{p},t)$ the Volkov solution [36] in the length gauge of an electron with canonical momentum $\mathbf{p}$:

$$|\psi_{\mathrm{V}}(\mathbf{p},t)\rangle = |\psi_{\mathrm{PW}}(\mathbf{p}+\mathbf{A}(t))\rangle \exp\left(-i\int^{t} dt'' \frac{(\mathbf{p}+\mathbf{A}(t''))^2}{2}\right). \qquad (17)$$

The Volkov solutions describe a free electron moving in the electric field of the laser only. The resulting integral over momenta in Eq. (11) can be approximated as described in the following.

In practice, saddle–point approximations are additionally applied to the integral in Eq. (11) [32, 37]. The most straightforward approach is to regard the matrix elements as slowly varying functions of the momentum $\mathbf{p}$ while the phase factor $\exp(-\mathrm{i}S)$ oscillates rapidly as a function of $\mathbf{p}$. One can then find the saddle–point momentum $\mathbf{p}_{\mathrm{s}}$ where the phase is stationary, *i.e.*, $\nabla_{\mathbf{p}} S(\mathbf{p},t',t)|_{\mathbf{p}=\mathbf{p}_{\mathrm{s}}} = 0$,

$$\mathbf{p}_{\mathrm{s}}(t',t) = -\int_{t'}^{t} \mathbf{A}(t'')/(t-t')dt''. \qquad (18)$$

The saddle–point approximation assumes that the integral is dominated by the integrand around $\mathbf{p}_{\mathrm{s}}$. Thus the matrix elements are evaluated at $\mathbf{p}_{\mathrm{s}}$, and the action is replaced by a second–order Taylor expansion in $\mathbf{p}$ around $\mathbf{p}_{\mathrm{s}}$. Carrying out the integration over momenta leads to [32, 37]

$$\mathbf{D}(t) = -\mathrm{i}\int_0^t \mathrm{d}t' \left[\frac{2\pi}{\epsilon + \mathrm{i}(t-t')}\right]^{3/2} \mathbf{d}_{\mathrm{r}}^{*}\big(\mathbf{p}_{\mathrm{s}}(t',t)+\mathbf{A}(t)\big)\, d_{\mathrm{i}}\big(\mathbf{p}_{\mathrm{s}}(t',t)+\mathbf{A}(t'),t'\big)$$
$$\times \exp\big(-\mathrm{i}S\big(\mathbf{p}_{\mathrm{s}}(t',t),t',t\big)\big) \quad + \quad \mathrm{c.c.} \qquad (19)$$

So far, we have introduced the standard form of the Lewenstein model, but alternatively one may calculate the dipole acceleration by directly evaluating the expectation value of the dipole acceleration operator $\nabla V + \mathbf{E}(t)$, without taking the double time derivative in Eq. (10). Or one may evaluate first the expectation value of the dipole momentum operator $\mathrm{i}\nabla$ and subsequently take one time derivative to arrive at the dipole acceleration. In Ref. [38], it was shown for $H_2^+$ that the third possibility, the *velocity form*, gives the best results in the sense that the shape of the resulting HHG spectra is closest to the spectra from the numerically exact solution of the TDSE. In the velocity form, one replaces in Eq. (19) the matrix element $\mathbf{d}_\mathrm{r}$ by the dipole–velocity matrix element

$$\mathbf{v}_\mathrm{r}(\mathbf{p}) = \langle \psi_\mathrm{PW}(\mathbf{p}) | \mathrm{i}\nabla | \psi_0 \rangle. \tag{20}$$

After this replacement, Eq. (19) yields not the expectation value of the dipole moment, but of the dipole velocity.

So far we have not discussed the question of length gauge versus velocity gauge. Although there is not a unique opinion in the literature about what gauge is most appropriate, previous work suggests that length gauge is preferable for atoms and small molecules [39, 40]. This seems to happen because in the length gauge the field–dressed ground state is similar to the field–free state used in the SFA. However, this statement does not hold for molecules at very large internuclear separations $R$, as was shown in Ref. [37]. In this case the length gauge leads to an unphysical increase of the cutoff frequency and the harmonic intensities as a function of $R$. Using velocity gauge in combination with a saddle–point approximation adapted to the presence of two centers leads instead to physically reasonable results. In velocity gauge, Eq. (11) is replaced by

$$\mathbf{D}(t) = -\mathrm{i} \int_0^t \mathrm{d}t' \int \mathrm{d}^3p \; \mathbf{d}_\mathrm{r}^*(\mathbf{p}) \, v_\mathrm{i}(\mathbf{p}, t') \, \exp\left(-\mathrm{i}S(\mathbf{p}, t', t)\right) \quad + \quad \text{c.c.} \tag{21}$$

with the velocity–gauge ionization matrix element

$$v_\mathrm{i}(\mathbf{p}, t) = \langle \psi_\mathrm{PW}(\mathbf{p}) | - \mathrm{i}\nabla \cdot \mathbf{A}(t) + A^2(t)/2 | \psi_0 \rangle. \tag{22}$$

The difference with respect to the length gauge is twofold: (i) the operator in the matrix element (22) is the one from the velocity–gauge Hamiltonian (2), and (ii) the momenta at which the ionization and recombination matrix elements in Eq. (21) are evaluated are the canonical "drift" momenta $\mathbf{p}$ instead of the instantaneous momenta $\mathbf{p} + \mathbf{A}(t)$. It is important not to confuse the velocity gauge of the Hamiltonian with the velocity form of the

recombination matrix element, Eq. (20). Both can be, but need not be, used in combination with each other.

The internuclear distances at which the unphysical behavior of the length gauge becomes relevant are of the order of $\pi\alpha$ where $\alpha$ is the classical oscillation amplitude of the electron in the laser field. These distances are much larger than typical equilibrium bondlengths. In the following we will concentrate on the case of small molecules and restrict ourselves to the length–gauge formulation.

### 2.4 *Odd and even harmonics*

For a monochromatic field or sufficiently long pulses, it follows from the photon picture that the harmonic frequencies are integer multiples of the laser frequency. In a typical experiment, one observes only the odd harmonics. This is the consequence of the inversion symmetry of the target gas. In simple terms, all half optical cycles of the driving laser field generate harmonics with the same intensities but with phase differences of $\pi$ relative to each other. The field of the XUV radiation obeys the symmetry

$$\mathbf{E}_{\mathrm{XUV}}(t + T/2) = -\mathbf{E}_{\mathrm{XUV}}(t), \tag{23}$$

where $T$ is the duration of the laser optical cycle. The Fourier spectrum of such a signal has only odd frequency components, *i.e.*, the peaks are separated by twice the laser photon frequency. Equation (23) is a special case of a dynamical symmetry in HHG. Reference [41] discusses the relation between dynamical symmetries and selection rules in HHG.

The existence of inversion symmetry is obvious for atoms which are spherically symmetric. It is also obvious for homonuclear diatomic molecules. In general, however, a molecule with fixed nuclear positions does not possess inversion symmetry. Nonetheless, in an experiment with randomly oriented molecules, one can consider the whole ensemble of molecules as being again inversion symmetric. The same statement remains true in experiments with laser–aligned molecules because alignment does not fix the orientation of the molecular axes. (Orientation refers to knowing also which atom is on which side.) Therefore, in practice one usually observes only odd harmonics when using long laser pulses.

Even harmonics could be measured with oriented heteronuclear molecules. A particularly interesting case of symmetry breaking occurs in an oriented HD molecule. For fixed nuclei, the electron dynamics is completely inversion symmetric. By including the coupling to the vibra-

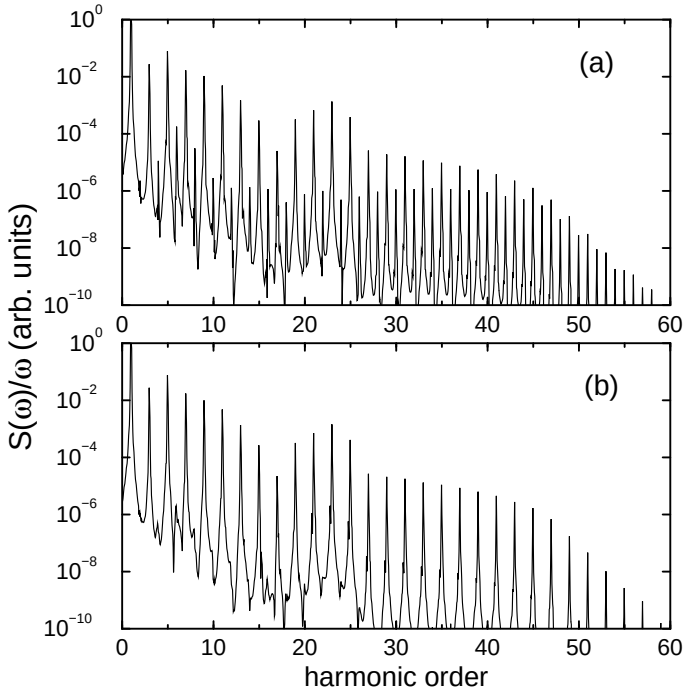


Fig. 3 (a) Harmonic spectrum generated from the 1D HD molecule driven by a laser field with peak intensity $10^{14}$ W/cm$^2$ and wavelength 770 nm. The plotted quantity is proportional to the number of emitted photons per frequency interval. (b) The same calculation for the 1D $H_2$ molecule. From [42], copyright 2001 by the American Physical Society.

tional degree of freedom, however, the molecule becomes asymmetric, giving rise to substantial even–harmonic generation [42]. This is an example of non-Born–Oppenheimer strong–field dynamics. Figure 3 compares HHG in one-dimensional $H_2$ and oriented one-dimensional HD. The spectra result from the numerical solution of the TDSE with three degrees of freedom: two electron coordinates and the internuclear distance. The spectra clearly show the absence of even harmonics in $H_2$ and their presence in oriented HD.

## 3 Influence of molecular structure on HHG

Equation (19) gives insight into the influence of molecular structure on HHG. The ground–state molecular orbital appears in the ionization and recombination matrix elements, $d_{\mathrm{i}}$ (or $v_{\mathrm{i}}$) and $\mathbf{d}_{\mathrm{r}}$ (or $\mathbf{v}_{\mathrm{r}}$). We will see that the effect of the two dependences is quite different: the ionization part influences mainly the overall efficiency of HHG and its dependence on the orientation of the molecular axis, while the recombination part additionally determines directly the shape of the HHG spectrum. Therefore, the recombination step may be considered the more important subject of investigation in molecular HHG. We will consider both points separately.

### 3.1 *Ionization step*

If ionization by an intense laser field takes place via tunneling, one may suspect that the electron loses to a certain extent its memory about its initial wave function on its way out of the molecule. Furthermore, one may think that the ionization probability is dictated mainly by the ionization potential of the system. However, one finds that the ionization yields can depend strongly on the molecular species and orientation. It is known from a series of experiments and theoretical works that strong–field ionization is suppressed in a number of molecules, when compared to ionization of a "companion" atom with similar ionization potential [43–55]. Since the literature does not seem to fully agree about the mechanisms responsible for these deviations, we will not further discuss ionization suppression in detail. We note, however, that the ionization step crucially influences the overall efficiency of HHG. We are predominantly interested in the momentum distributions of electron wave packets after ionization, since they will influence the shape of the HHG spectra. Often, this distribution is found to be rather insensitive to the molecular structure, e.g. in the comparison of aligned $N_2$ molecules at different angles [56]. On the other hand, there is an important exception in the case of molecular orbitals with mirror antisymmetry. If the electric field of the laser pulse points parallel to a nodal plane, then the antisymmetry is conserved, and there are no electrons moving strictly parallel to the field. Rather, the electron always exhibits a lateral drift motion, which makes the usual three–step model inapplicable (since it assumes zero initial velocity). The lateral drift strongly suppresses recollisions, and the efficiency of HHG is reduced. In this exceptional case the use of elliptical polarization can enhance HHG by compensating the

drift. We illustrate this behavior [57] using the example of the first excited state of the $H_2^+$ molecular ion, which possesses a nodal plane perpendicular to the molecular axis. Instead of the three-dimensional system, we consider a 2D model system with the binding potential

$$V(x,y) = -\sum_{k=1,2} \frac{1}{\sqrt{(x-x_k)^2 + (y-y_k)^2 + 0.5}}. \tag{24}$$

The soft–core potential with the softening parameter 0.5 avoids the numerical difficulties of a Coulomb singularity. It is also physically more applicable than a bare $1/r$ Coulomb potential in 2D, because it mimics the fact that in 3D, the electron has more available "space" to bypass the nucleus. The soft–core potential can be viewed as an average of the 3D potential over the third dimension [58]. The TDSE for one electron in the potential (24) plus the interaction with a 780 nm laser pulse with intensity $4\times10^{14}\,\mathrm{W/cm^2}$ is solved numerically by means of the split–operator method [59]. We consider the special case that the molecule is aligned perpendicular to the major axis of the elliptical laser polarization since this means that the electric field points along the nodal plane in the limit of linear polarization. The intensities of the harmonic orders 31, 41, 51, and 61 are shown in Fig. 4 as a function of laser ellipticity. The maximum at non-zero ellipticity is a clear signature of the orbital antisymmetry. It is apparent that the saddle–point version of the strong–field approximation, Eq. (19) cannot explain the non-zero harmonic intensity for linear polarization, since the saddle–point momentum is parallel to the polarization axis and therefore the ionization and recombination matrix elements vanish due to the orbital antisymmetry. This can be interpreted such that the lowest–order saddle point approximation is not sufficient to replace the integration over momenta in the SFA expression.

Nodal planes induce a strong dependence of the efficiency of HHG on the alignment of the molecule. We note that the antisymmetry leads also to strong suppression of the total ionization probability when the electric field points along a nodal plane so that the orientation dependence of the ionization probability gives a qualitative image of the initial electron orbital [60].

In the example above there are two physical ingredients, namely a nodal plane and the use of ellipticity, that are both detrimental to the HHG efficiency if they are taken by themselves. In the combination of both, however, they can compensate each other. In the same spirit, it has recently been proposed to compensate the lateral drift from the nodal plane by a non-dipole effect [61, 62]. It is well known that the effect of the magnetic field

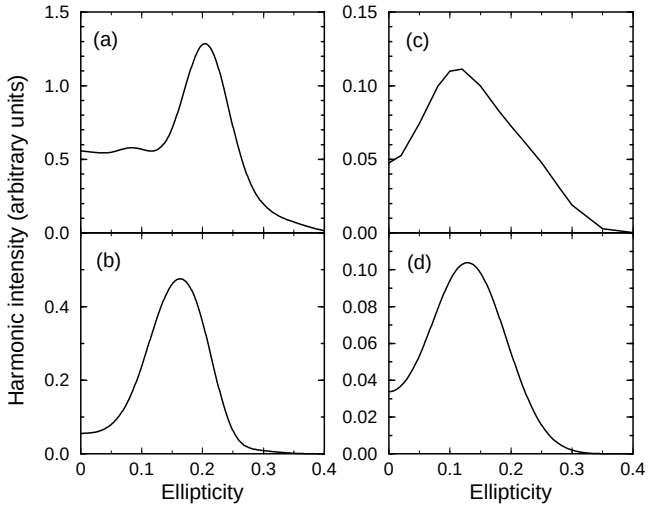


Fig. 4 Ellipticity dependence of the harmonic intensities for the antisymmetric 1st excited state of 2D $H_2^+$, oriented perpendicular to the laser field. Laser pulses with 780 nm wavelength and intensity $4\times10^{14}$ W/cm$^2$ are used. (a) 31st, (b) 41st, (c) 51st, (d) 61st harmonic. Data from [57].

of a laser pulse is to push the freed electron into the laser propagation direction and thereby to reduce the recollision probability [63, 64]. For suitable alignment of the molecule, the magnetically induced drift partially counteracts the drift due to the orbital structure. To be precise, the compensation is effective when the laser propagation axis is perpendicular to the nodal plane.

### 3.2 *Recombination step*

In the framework of the SFA, the recombination step affects HHG through the recombination matrix element. The essential difference with respect to the ionization step, however, is that the returning electron momenta are significantly higher than the initial momenta. The de Broglie wavelength of the electron can be comparable to the internuclear distance. Consequently, one may expect interference effects in HHG from a diatomic molecule, in analogy to Young's double slit interference. We demonstrate this behavior by investigating once more the 2D model of $H_2^+$ that we introduced in the previous section. The initial state is now taken to be the symmetric ground state. The resulting spectra for 2D $H_2^+$ aligned at various different angles

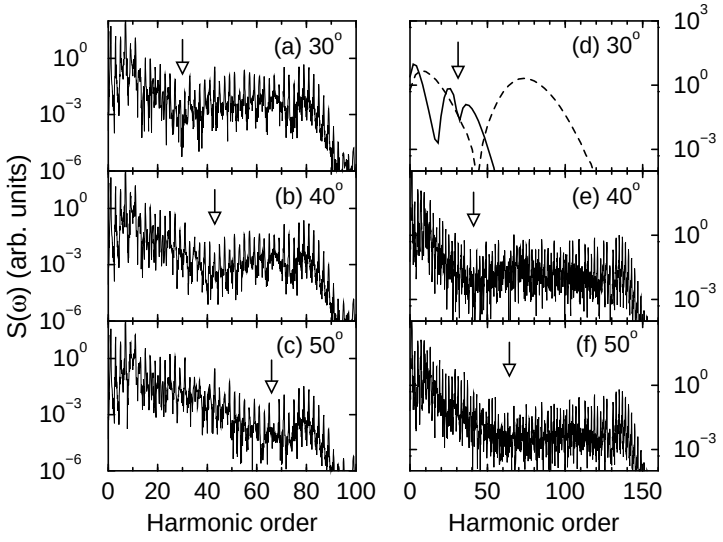


Fig. 5 Spectra of harmonics polarized parallel to the laser polarization direction for 2D $H_2^+$ in 780 nm laser pulses, aligned at various angles as indicated. Left panels: laser pulses with intensity $5\times10^{14}$ W/cm$^2$. Panel (d): field–free simulation for recolliding wave packets with energies corresponding to the 31st harmonic (solid line) and 75th harmonic (dashed line). Panels (e),(f): laser pulses with intensity $1\times10^{15}$ W/cm$^2$. From [15], copyright 2002 by the American Physical Society.

with respect to the polarization axis of a linearly polarized 780 nm laser pulse are shown in Fig. 5. Two different laser intensities are compared. Furthermore, panel (d) of the figure shows the result of a laser–field–free simulation where the initial state is the superposition of the ground state with an incoming electron wave packet, the momentum of which is chosen such that it corresponds to the 31st or 75th harmonic, respectively. In all cases, we observe a clear suppression of harmonic emission around a harmonic frequency that depends on the orientation angle but is independent of the laser parameters. The same observation can be made in the results of time–dependent Hartree–Fock calculations for the case of a 2D $H_2$. The binding potential is the same as given by Eq. (24), but with softening parameter 0.41 instead of 0.5. Additionally, the $H_2$ model assumes a mean–field potential

$$V_{\rm ee}(\mathbf{r}) = \int \frac{|\Psi(\mathbf{r}',t)|^2 d^2r'}{\sqrt{(\mathbf{r}-\mathbf{r}')^2+0.36}} \qquad (25)$$

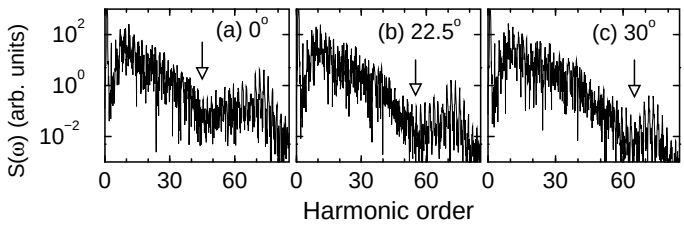


Fig. 6 Spectra of harmonics polarized parallel to the laser polarization direction for 2D $H_2$ in 780 nm laser pulses with intensity $5\times10^{14}$ W/cm$^2$. The alignment angle of the molecule is as indicated. From [15], copyright 2002 by the American Physical Society.

describing the electron–electron interaction. The results for various orientations of this model molecule are shown in Fig. 6. Similar to $H_2^+$, the HHG spectra exhibit a minimum moving to higher harmonic orders with increasing angle between molecule and laser field.

HHG can be used for attosecond–pulse generation by superposition of harmonics with different frequencies. The duration and shape of attosecond pulses depend on the phases of the different harmonics. The harmonic phase can be calculated simply as the phase of the complex Fourier transformed acceleration, $\mathbf{a}(\omega)$. Figure 7 compares the orientation dependences of the harmonic intensity and of the harmonic phase for the 43rd harmonic in 2D $H_2^+$. It is apparent that the minimum in the harmonic yield coincides with a jump of the phase about $\pi$. Except for the jump, the phase is approximately constant. This suggests that the complex harmonic amplitude $\mathbf{a}(\omega)$ goes through zero at a certain angle of orientation.

If the observed minimum is due to destructive double–slit type interference, we can write the interference conditions in simple form. Assuming that the contributions from the two centers interfere with a phase difference determined by the de Broglie wavelength $\lambda$ of the returning electron and the projection of the internuclear distance on the laser polarization axis, $R\cos\theta$ predicts interference minima at

$$R\cos\theta = (2n+1)\frac{\lambda}{2}, \quad n = 0, 1, 2, \ldots, \tag{26}$$

while interference maxima are expected for

$$R\cos\theta = n\lambda, \quad n = 1, 2, \ldots. \tag{27}$$

This model has recently been named the two–point emitter model. In order to corroborate the idea of two–center interference, data from extensive simulations of $H_2^+$ and $H_2$ was collected [65], and the positions of the minima

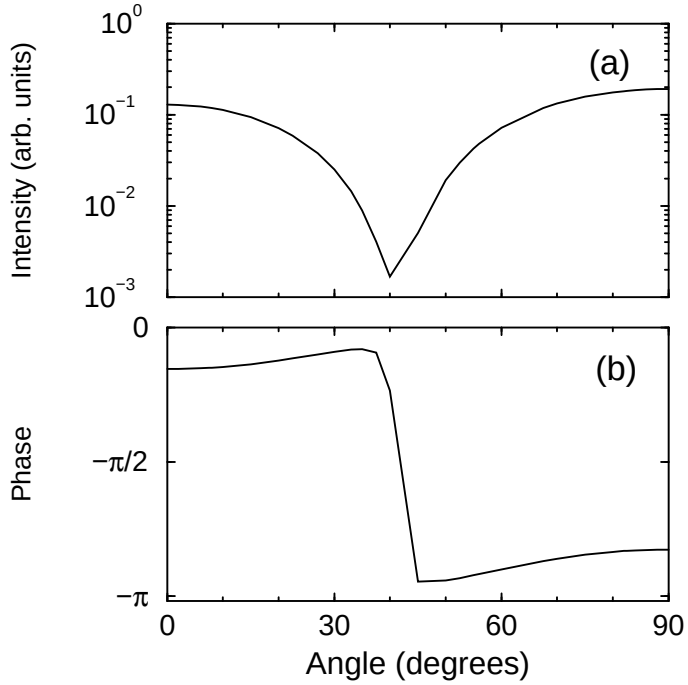


Fig. 7 Orientation dependence of the 43rd harmonic for 2D $H_2^+$ in a 780 nm laser pulse with intensity $5\times10^{14}$ W/cm$^2$. (a) Harmonic intensity; (b) harmonic phase. From [65], copyright 2002 by the American Physical Society.

and maxima found in the spectra and in the orientation dependences were compared with the simple double–slit formulas. The result is plotted in Fig. 8. The straight lines show the predictions of the formulas (26),(27). The minima and maxima found from the numerical TDSE calculations are plotted as data points. For the conversion of harmonic frequencies $\omega$ to the electron wavelength $\lambda = 2\pi/k$, a heuristically corrected relation is used,

$$\frac{k^2}{2} = \omega, \tag{28}$$

instead of the usual relation $k^2/2 + I_\mathrm{p} = \omega$ that emerges from the SFA or simple man's model. The idea behind this correction is that the interference is not determined by the wavelength corresponding to the asymptotic energy of the electron far away from the core, $E_\mathrm{asympt} = \omega - I_\mathrm{p}$. The interference is dictated by the wavelength in the core region, where the electron is faster due to the attractive long–range binding potential. The energy

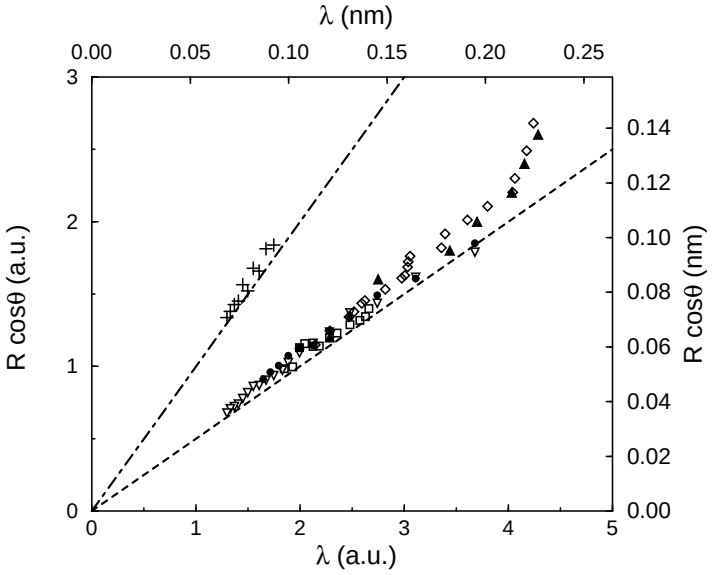


Fig. 8 Projection of the internuclear distance on the polarization axis, $R\cos\theta$, versus the de Broglie wavelength of the recolliding electron for which the harmonic yield is minimal (lower points) or maximal (upper points). The wavelength is calculated as explained in the text. Straight lines, two–point emitter model given by Eqs. (26),(27). From [65], copyright 2002 by the American Physical Society.

amount $I_{\rm p}$ appears to be the natural scale of the correction. We observe in Fig. 8 that the numerical results agree well with the two–point emitter model when we use equation (28). For a discussion of this "dispersion relation" in the context of atomic HHG, see Ref. [66].

The 2D calculations for $H_2^+$ were followed by 3D calculations that led to the same findings: in Ref. [67], a 3D soft–core potential was employed in TDSE simulations on a numerical grid, while later in Refs. [68, 69] a basis–set expansion was applied to the TDSE for the bare two–center Coulomb potential of $H_2^+$.

In the discussion so far, the two–center interference is a phenomenon that we expect from the intuitive picture that the recolliding electron finds two possible sites for recombination. One can derive the two–center interference from the SFA if one uses (i) the velocity form of the recombination matrix element and (ii) a linear combination of atomic orbitals (LCAO) for the initial electronic wave function, *i.e.*,

$$\Psi_0(\mathbf{r}) \sim \varphi_0(\mathbf{r}-\mathbf{R}/2) + \varphi_0(\mathbf{r}+\mathbf{R}/2). \tag{29}$$

One obtains for the matrix element

$$\langle \exp(\mathrm{i}\mathbf{k}\cdot\mathbf{r})|\mathrm{i}\nabla|\Psi_0\rangle \sim 2\,\cos(\mathbf{k}\cdot\mathbf{R}/2)\,\langle \exp(\mathrm{i}\mathbf{k}\cdot\mathbf{r})|\mathrm{i}\nabla|\varphi_0\rangle. \qquad (30)$$

The function $\cos(\mathbf{k}\cdot\mathbf{R}/2)$ expresses explicitly the two–center interference and is consistent with the two–point emitter model, except for the different "dispersion relation" in the SFA. References [69, 70] compare dipole and acceleration forms and show that the two–point emitter formulas follow from the acceleration form, if large internuclear distance is assumed as an additional approximation.

If the molecular orbital is an LCAO with opposite signs of the atomic orbitals, *i.e.*,

$$\Psi_0(\mathbf{r}) \sim \varphi_0(\mathbf{r}-\mathbf{R}/2) - \varphi_0(\mathbf{r}+\mathbf{R}/2), \qquad (31)$$

one can show immediately that

$$\langle \exp(\mathrm{i}\mathbf{k}\cdot\mathbf{r})|\mathrm{i}\nabla|\Psi_0\rangle \sim 2\mathrm{i}\,\sin(\mathbf{k}\cdot\mathbf{R}/2)\,\langle \exp(\mathrm{i}\mathbf{k}\cdot\mathbf{r})|\mathrm{i}\nabla|\varphi_0\rangle. \qquad (32)$$

This means that the interference minima and maxima are now interchanged as compared to the case of Eq. (29) [65]. It is important to note that the form of Eq. (31) does *not* imply that the orbital is antibonding or antisymmetric with respect to a mirror or inversion operation. Rather, the two atomic orbitals that are added with opposite signs in Eq. (31) are spatially translated relative to each other. This point has sometimes led to confusion in the literature; for clarification see also Refs. [71, 72]. An instructive example is the $\sigma_\mathrm{g}$ valence orbital of the $N_2$ molecule. It is a symmetric orbital (with respect to both inversion and reflection), but in a very rough LCAO approximation, it would be the sum of two atomic p-orbitals, added with *opposite signs*. Therefore, the expected interference behavior is different from $H_2$ and $H_2^+$. The simple LCAO orbital, however, is not a realistic approximation for the $N_2$ orbital, since atomic s-orbitals contribute about 30% to the molecular orbital. The two s-orbitals have to be added with equal signs in order to give a symmetric molecular orbital. The two types of interference (corresponding to LCAOs with either plus or minus sign) are thus mixed together in one molecular orbital. As a result, there is no simple double–slit type interference in $N_2$ [73]. This is confirmed by experiments on aligned $N_2$ [16, 74].

Next, we consider the carbon dioxide molecule $CO_2$, which has the linear structure OCO. The doubly degenerate valence orbital has $\pi_\mathrm{g}$ symmetry with two nodal planes, one along the molecular axis, one perpendicular to it. The orbital can be well approximated by two atomic p-orbitals with

opposite signs centered at the oxygen atoms. Therefore, two–center interference is expected for HHG from $CO_2$, and this is confirmed by experiments on aligned $CO_2$ [17, 75]. Kanai *et al.* have proved that the minimum observed in the HHG spectrum of $CO_2$ must be due to the recombination step in the three–step model by measuring simultaneously the harmonic intensity and the ionization yield. They found that the suppression of the harmonic intensity coincides with an increased ionization yield, ruling out the possibility that the suppression is caused by the ionization step.

Itatani *et al.* [16] proposed that the orbital dependence of HHG can be exploited to retrieve the orbital from the measured harmonics. This requires measurements of the HHG spectra for many different orientation angles of the molecule. One assumes that the HHG spectrum can be expressed as a product of a prefactor and the modulus squared of the recombination matrix element $\mathbf{d}(\omega, \theta)$,

$$S(\omega, \theta) \sim \omega^4 |a(\omega)\mathbf{d}(\omega, \theta)|^2. \tag{33}$$

By measuring the harmonic spectrum for a reference atom with known orbital, one can obtain the function $|a(\omega)|^2$. Assuming that the ionization and acceleration steps in the molecule are similar to the atom, one uses the same prefactor for the molecule so that from the measured molecular HHG spectra and Eq. (33), one obtains $|\mathbf{d}(\omega, \theta)|^2$. Assuming or measuring the phase of $\mathbf{d}$, one knows the complex values $|\mathbf{d}(\omega, \theta)$. One can then obtain the orbital by inverse Fourier transformation. In Ref. [16] the phase was assumed to behave according to the findings of Refs. [15, 65], namely that a phase jump by $\pi$ occurs where the harmonic intensity exhibits a minimum (see Fig. 7). A direct measurement of the harmonic phase seems possible [7, 76, 77], but one must then also know the phase of the quantity $a(\omega)$ to obtain the phase of the transition matrix element $\mathbf{d}$. Reference [16] presents the result of the tomographic procedure for the $N_2$ molecule and finds good qualitative agreement with an ab initio orbital. Further work discussing multielectron effects is found in Refs. [78, 79]. Application to other molecules is work in progress. Complications arise for orbitals with nodal planes for the reasons explained in the previous section. At present it seems that for such orbitals, one has to prescribe the nodal planes by hand in order to make the tomographic reconstruction work.

## 4 Dynamical effects

In the preceding sections, we have ignored the nuclear motion in laser–driven molecules. This is expected to be a good approximation for many molecules (including for example $N_2$) in ultrashort few–cycle pulses, because the vibrational and rotational period is long compared to the pulse duration. The only expected effect is that one should average the results over the distribution of internuclear distances and orientations. In a typical experiment, this is the distribution corresponding to the vibrational ground state and random alignment of the molecular axes. However, one can also employ a prepulse that creates a rotational or a vibrational wave packet which would then determine the distribution at the time of arrival of the strong driving pulse generating the harmonics. Note that the coherent superposition of the complex harmonic amplitudes for different molecular orientations/geometries has to be taken, rather than an incoherent summation of harmonic intensities [80].

The assumption of frozen nuclei does not hold for very light molecule. In particular, we expect that nuclear motion takes places during the action of the driving pulse for molecules with bound hydrogen atoms. This includes of course hydrogen molecules, but also many other important species such as water or methane. The rotational motion can still be considered frozen during the laser pulse, but the vibrational period can be comparable to the pulse duration. We focus here on the possibility that the ionization of the molecule creates a vibrational wave packet in the molecular ion. If there is significant wave–packet motion between the ionization and recombination steps in the HHG process, we expect an influence on the HHG spectra. Since the vibrational wave packet is launched together with the continuum electron wave packet, we have a *correlated wave–packet motion*.

Effects of nuclear motion have been seen in several simulations of HHG, in which the TDSE for $H_2^+$ was solved numerically [81–84]. The first demonstration of the effect of correlated nuclear and electronic wave packets in HHG, however, was seen in TDSE calculations for two–dimensional $H_2$ and $D_2$ model molecules [85], incorporating one–dimensional vibrational motion and two–dimensional electron motion. Figure 9 shows the ratio of the harmonics in $D_2$ and $H_2$ as well as the ratio $T_2/H_2$ for two different laser wavelengths, namely 780 nm and 1200 nm. The molecules are aligned perpendicular to the electric field of the laser pulse, except for the stars in Fig. 9(a), which refer to randomly aligned molecules. We see clearly that the heavier isotopes generate harmonics more efficiently. For example, the

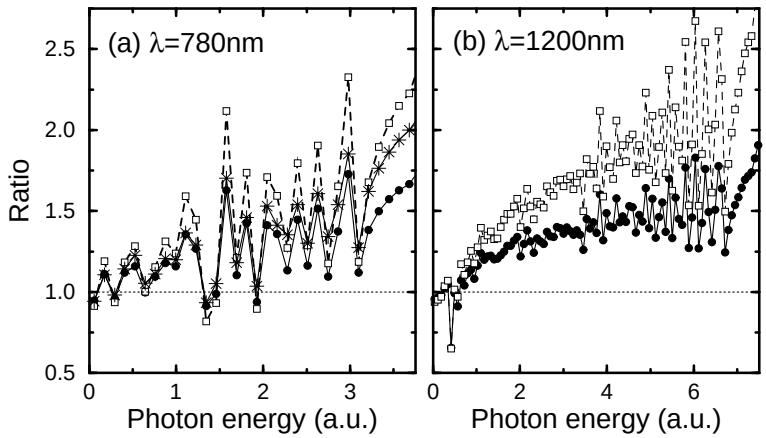


Fig. 9 Ratio of harmonics in different isotopes for 780 nm and 1200 nm laser pulses as indicated. Full circles, ratio $D_2/H_2$; open squares, ratio $T_2/H_2$ (molecules aligned perpendicular to the field). Stars in the left panel, ratio $D_2/H_2$ calculated for random alignment. From [85], copyright 2005 by the American Physical Society.

ratio $D_2/H_2$ is almost always greater than one. The ratio tends to increase as a function of harmonic order. At least for this set of parameters, there is not a big difference between perpendicular and random alignment. We can understand the result in terms of the three–step model. In the time between ionization and recombination, the ionized molecule expands. This occurs faster in the lighter isotope $H_2$ because of the smaller reduced nuclear mass. Recombination must lead back into the initial state, *i.e.* into the vibronic ground state with internuclear distances near the equilibrium distance. The probability of this transition is reduced when the mean internuclear distance of the wave packet in the molecular ion becomes larger. The suppression is therefore more pronounced in the lighter isotope. We can also interpret the increase of the ratio with harmonic order, since according to the three–step model, the higher harmonics are generated by longer electron travel times, see Eq. (9), leaving more time for the nuclear wave–packet dynamics. The physical process is illustrated in Fig. 10. It shows the ground–state Born–Oppenheimer (BO) potentials of $H_2$ and $H_2^+$ and the vibrational wave–packet dynamics in the $H_2^+$ potential.

To understand this effect quantitatively, we introduce the strong–field approximation for molecules including the vibrational dynamics of the molecular ion after ionization [85–87]. One obtains the time–dependent

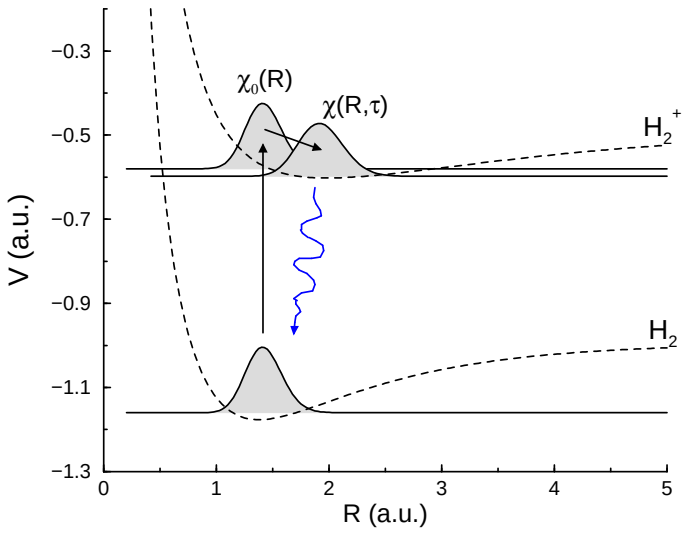


Fig. 10 Illustration of the harmonic–generation process in $H_2$. Shown are the Born–Oppenheimer potentials for the electronic ground states of $H_2$ and $H_2^+$ and the wave–packet evolution in the $H_2^+$ potential after ionization of $H_2$.

dipole moment

$$\begin{aligned}\mathbf{D}(t) \;&= -2\mathrm{i}\int_0^t dt' \left(\frac{2\pi}{\mathrm{i}(t-t')+\epsilon}\right)^{3/2} \int_0^\infty dR\, \chi_0^*(R)\, \mathbf{d}_\mathrm{r}^*\big(\mathbf{p}_\mathrm{s}(t',t)+\mathbf{A}(t)\big) \\ &\quad \times \exp\big(-\mathrm{i}S(t',t)\big)\hat{U}_R(t-t')\, d_\mathrm{i}\big(\mathbf{p}_\mathrm{s}(t',t)+\mathbf{A}(t'),t'\big)\,\chi_0(R) \\ &\quad + \text{c.c.}, \end{aligned} \tag{34}$$

where the saddle–point approximation for the integration over momenta has already been carried out. This equation corrects typographical errors in equation (3) of [87]. $\chi_0(R)$ denotes the vibrational ground state of $H_2$, and the ionization and recombination matrix elements are

$$d_\mathrm{i}(\mathbf{p},t) = \langle\psi_\mathrm{PW}(\mathbf{p})\psi_R^+|E(t)z|\psi_R\rangle_{\mathbf{r}\mathbf{r}'}, \tag{35}$$

$$\mathbf{d}_\mathrm{r}(\mathbf{p}) = \langle\psi_\mathrm{PW}(\mathbf{p})\psi_R^+|-\mathbf{r}|\psi_R\rangle_{\mathbf{r}\mathbf{r}'}, \tag{36}$$

with $\psi_R(\mathbf{r},\mathbf{r}')$ and $\psi_R^+(\mathbf{r}')$ being the electronic BO states in $H_2$ and $H_2^+$. The time–evolution operator $\hat{U}_R(t-t')$ propagates the vibrational wave packet in the BO potential of the molecular ion, according to the one–dimensional TDSE for the internuclear distance. The prefactor 2 in equation (34) stands for the two electrons in $H_2$. Exchange terms [88, 78, 79] due to the two–electron nature of the system are neglected in Eq. (34).

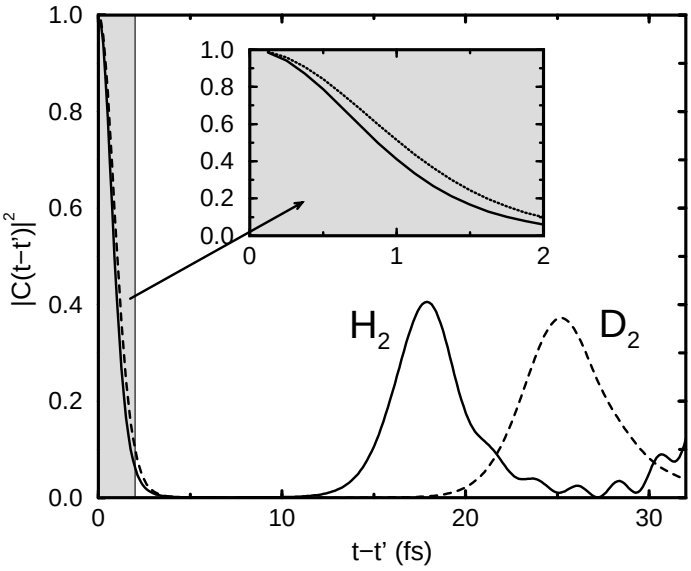


Fig. 11 Modulus squared of the vibrational autocorrelation functions for the wave–packet evolution in $H_2^+$ (solid) and $D_2^+$ (dashed). The initial wave packet is the vibrational ground state of the neutral molecule.

If one could neglect the dependence of the matrix elements on $R$, the only dependences on $R$ in the SFA integral would be in $\chi_0(R)$ and in the time–evolution operator. This leads a simple expression for the SFA integral where only the vibrational autocorrelation function

$$C(\tau) = \int_0^\infty dR\, \chi^*(R,0)\chi(R,\tau) \tag{37}$$

appears in addition to the SFA expression for atoms [85]. The autocorrelation function is the overlap of the evolved vibrational wave packet at the time of recombination with the initial wave packet at the time of ionization. If a harmonic is considered to be generated by only one pair of ionization time $t'$ and recombination time $t$, then the harmonic intensity is proportional to the modulus squared of the autocorrelation function, shown in Fig. 11 as a function of the travel time. The maxima at 18 fs for $H_2^+$ and 25 fs for $D_2^+$ correspond to the vibrational periods of these molecular ions. The typical electron travel times in HHG with 800 nm light, however, are below 2 fs since the optical period is only 2.7 fs. The inset shows $|C(\tau)|^2$ at such short times. In this region, the autocorrelation of $D_2^+$ is always greater

than the one of $H_2^+$, because of the faster dynamics in the latter. The ratio of the two curves is in good but not perfect agreement with the ratio of harmonics in $D_2$ and $H_2$ as calculated from the TDSE, see Fig. 3 in Ref. [85]. The remaining discrepancies can be due to differences of the initial wave packet from the vibrational ground state $\chi_0$, caused by the $R$–dependent ionization probability [89]. Another point is the slightly different ionization probabilities in $H_2$ and $D_2$, which can modify the harmonic ratios [87].

The experiment of Ref. [18] confirms that $D_2$ produces more intense harmonics than $H_2$. Also, the experimental ratio increases as a function of harmonic order. In Refs. [85, 18] it has been demonstrated that the time evolution of the internuclear distance can be reconstructed from the measured ratios by employing an iterative genetic algorithm that optimizes the time evolution such that the ratio of autocorrelation functions matches the measured ratio of harmonics.

The use of the simple autocorrelation function amounts to ignoring the two–center interference. The inclusion of the dependence of the matrix elements on the internuclear distance recovers the two–center interference effect, see the discussion in Refs. [18, 87]. The evaluation of the strong–field approximation then reveals an additional modulation in the ratio $D_2/H_2$ which is due to the fact that the destructive interference minimum is reached at different times in $D_2$ and $H_2$. This follows from the different speeds of wave–packet motion. Subject of current investigations is the question whether the time–evolution of the internuclear evolution after ionization can be directly imaged from the observation of this two–center interference. It is not directly obvious yet, how to disentangle the interference from the effect due to the wave–packet overlap described above.

## 5 Conclusions

We have given an introduction into the physical phenomena taking place in high–order harmonic generation with molecules. We have focused on three points: (i) the influence of molecular orbital structure on the ionization characteristics, (ii) the influence of the orbital on recombination (with two–center interference being the simplified perspective on this dependence in diatomic molecules), and (iii) the effects of vibrational motion on HHG. Molecular HHG is currently intensively studied by several experimental and theoretical groups, since it promises new approaches to molecular imaging, see also the review article Ref. [90]. Furthermore, molecules offer the pos-

sibility to manipulate the harmonic phase in a more flexible way than in atomic HHG. This may open new possibilities for attosecond–pulse shaping and for quasi phase matching.

## Acknowledgments

We thank J. Marangos and D. Villeneuve for valuable discussions, and we gratefully acknowledge discussions within the NSERC SRO network 'Controlled electron re-scattering: femtosecond, sub-angstrom imaging of single molecules'. This work was supported in part by the Deutsche Forschungsgemeinschaft.

## References

[1] McPherson, A., *et al.* (1987). *J. Opt. Soc. Am. B* **4**, 595.
[2] L'Huillier, A., Schafer, K. J., and Kulander, K. C. (1991). *J. Phys. B* **24**, 3315.
[3] Baeva, T., Gordienko, S., Pukhov, A. (2006). *Phys. Rev. E* **74**, 046404.
[4] Kulander, K. C., and Schafer, K. J., and Krause, J. L. (1993). In *Proceedings of the Workshop, Super Intense Laser Atom Physics (SILAP) III*, edited by B. Piraux, A. L'Huillier, and J. Rzążewski (Plenum Press, New York).
[5] Corkum, P. B. (1993). *Phys. Rev. Lett.*, **71**, 1994.
[6] Paul, P. M., Toma, E. S., Breger, P., Mullot, G., Augé, F., Balcou, P., Muller, H. G., and Agostini, P. (2001). *Science* **292**, 1689.
[7] Mairesse, Y., *et al.* (2003). *Science* **302**, 1540.
[8] Tzallas, P., Charalambidis, D., Papadogiannis, N. A., Witte, K., and Tsakiris, G. D. (2003). *Nature* **426**, 267.
[9] Drescher, M., Hentschel, M., Kienberger, R., Tempea, G., Spielmann, C., Reider, G. A., Corkum, P. B., and Krausz, F. (2001). *Science* **291** 1923.
[10] Hentschel, M., *et al.* (2001). *Nature* **414**, 509.
[11] Agostini, P., and DiMauro, L. F. (2004). *Rep. Prog. Phys.* **67**, 813.
[12] Scrinzi, A., Ivanov, M. Y., Kienberger, R., and Villeneuve, D. M. (2006). *J. Phys. B* **39**, R1.
[13] Sansone, G., *et al.* (2006). *Science* **314**, 443.
[14] Zewail, A. H. (2000). *J. Phys. Chem. A* **104**, 5660.
[15] Lein, M., Hay, N., Velotta, R., Marangos, J. P., and Knight, P. L. (2002). *Phys. Rev. Lett.* **88**, 183903.
[16] Itatani, J., *et al.* (2004). *Nature* **432**, 867.
[17] Kanai, T., Minemoto, S., and Sakai, H. (2005). *Nature* **435**, 470.
[18] Baker, S., *et al.* (2006). *Science* **312**, 424.
[19] Velotta, R., Hay, N., Mason, M. B., Castillejo, M., and Marangos, J. P. (2001). *Phys. Rev. Lett.* **87**, 183901.

[20] Itatani, J., Zeidler, D., Levesque, J., Spanner, M., Villeneuve, D. M., and Corkum, P. B. (2005). *Phys. Rev. Lett.* **94**, 123902.
[21] Niikura, H., *et al.* (2002). *Nature* **417**, 917.
[22] Niikura, H., *et al.* (2003). *Nature* **421**, 826.
[23] Bloch, F., and Nordsieck, A. (1937). *Phys. Rev.* **52**, 54.
[24] Pauli, W., and Fierz, M. (1938). *Nuovo Cimento* **15**, 167.
[25] Kramers, H. A. (1956). *Collected Scientific Papers* (North Holland, Amsterdam).
[26] Henneberger, W. C. (1968). *Phys. Rev. Lett.* **21**, 838.
[27] Faisal, F. H. M. (1973). *J. Phys. B* **6**, L89.
[28] Sundaram, B., and Milonni, P. W. (1990). *Phys. Rev. A* **41**, 6571.
[29] Eberly, J. H., and Fedorov, M. V. (1992). *Phys. Rev. A* **45**, 4706.
[30] Burnett, K., Reed, V. C., Cooper, J. and Knight, P. L. (1992). *Phys. Rev. A* **45**, 3347.
[31] Lappas, D. G., Fedorov, M. V., and Eberly, J. H. (1993). *Phys. Rev. A* **47**, 1327.
[32] Lewenstein, M., Balcou, P., Ivanov, M. Y., L'Huillier, A., and Corkum, P. B. (1994). *Phys. Rev. A* **49**, 2117.
[33] Salières, P., L'Huillier, A., and Lewenstein, M. (1995). *Phys. Rev. Lett.* **74**, 3776.
[34] Antoine, P., L'Huillier, A., and Lewenstein, M. (1996). *Phys. Rev. Lett.* **77**, 1234.
[35] Balcou, P., Salières, P., L'Huillier, A., and Lewenstein, M. (1997). *Phys. Rev. A* **55**, 3204.
[36] Wolkow, D. M. (1935). *Z. Physik* **94**, 250.
[37] Chirilă, C. C., and Lein, M. (2006). *Phys. Rev. A* **73**, 023410.
[38] Chirilă, C. C., and Lein, M. (2007). *J. Mod. Opt.* **54**, 1039.
[39] Bauer, D., and Milošević, D. B., and Becker, W. (2005). *Phys. Rev. A* **72**, 023415 (2005).
[40] Kjeldsen, T. K., and Madsen, L. B. (2004). *J. Phys. B* **37**, 2033 (2004).
[41] Alon, O. E., Averbukh, V., and Moiseyev, N. (1998). *Phys. Rev. Lett.* **80**, 3743.
[42] Kreibich, T., Lein, M., Engel, V., and Gross, E. K. U. (2001). *Phys. Rev. Lett.* **87**, 103901.
[43] Talebpour, A., Chien, C.-Y., and Chin, S. L. (1996). *J. Phys. B* **29**, L677.
[44] Talebpour, A., Larochelle, S., and Chin S. L. (1998), *J. Phys. B* **31**, L49.
[45] Guo, C., Li, M., Nibarger, J. P., and Gibson, G. N. (1998). *Phys. Rev. A* **58**, R4271.
[46] Wells, E., DeWitt, M. J., and Jones, R. R. (2002). *Phys. Rev. A* **66**, 013409.
[47] Hankin, S. M., Villeneuve, D. M., Corkum, P. B., and Rayner, D. M. (2000). *Phys. Rev. Lett.* **84**, 5082.
[48] Benis, E. P.,*et al.* (2004). *Phys. Rev. A* **70**, 025401.
[49] DeWitt, M. J., and Levis, R. J. (1998). *J. Chem. Phys.* **108**, 7739.
[50] Saenz, A. (2000). *J. Phys. B* **33**, 4365.
[51] Guo, C. (2000). *Phys. Rev. Lett.* **85**, 2276.
[52] Muth-Böhm, J., Becker, A., and Faisal, F. H. M. (2000). *Phys. Rev. Lett.*,

**85**, 2280.
[53] Campbell, E. E. B., Hoffmann, K., Rottke, H., and Hertel, I. V. (2001). *J. Chem. Phys.* **114**, 1716.
[54] Tchaplyguine, M., *et al.* (2000). *J. Chem. Phys.* **112**, 2781.
[55] Bhardwaj, V. R., Corkum, P. B., and Rayner, D. M. (2003). *Phys. Rev. Lett.* **91**, 203004.
[56] Zeidler, D., Bardon, A. B., Staudte, A., Villeneuve, D. M., Dörner, R., and Corkum, P. B. (2006). *J. Phys. B* **39**, L159.
[57] Lein, M., (2003). *J. Phys. B* **36**, L155.
[58] Lein, M., Gross, E. K. U., and Engel, V. (2000). *J. Phys. B* **33**, 433.
[59] Feit, M. D., Fleck, J. A., Jr., and Steiger, A. (1982). *J. Comput. Phys.* 47, 412.
[60] Lagmago Kamta, G., and Bandrauk, A. D. (2006). *Phys. Rev. A* **74**, 033415.
[61] Fischer, R., Lein, M., and Keitel, C. H. (2006). *Phys. Rev. Lett.* **97**, 143901.
[62] Fischer, R., Lein, M., and Keitel, C. H. (2007). *J. Phys. B* **40**, F113.
[63] Walser, M. W., Keitel, C. H., Scrinzi, A., and Brabec, T. (2000). *Phys. Rev. Lett.* **85**, 5082.
[64] Kylstra, N. J., Potvliege, R. M., and Joachain, C. J. (2001). *J. Phys. B* **34**, L55.
[65] Lein, M., Hay, N., Velotta, R., Marangos, J. P., and Knight, P. L. (2002). *Phys. Rev. A* **66**, 023805.
[66] Levesque, J., Zeidler, D., Marangos, J. P., Corkum, P. B., and Villeneuve, D. M. (2007). *Phys. Rev. Lett.* **98**, 183903.
[67] Lein, M., Corso, P. P., Marangos, J. P. and Knight, P. L. (2003). *Phys. Rev. A* **67**, 023819.
[68] Lagmago Kamta, G., and Bandrauk, A. D. (2004). *Phys. Rev. A* **70**, 011404(R).
[69] Lagmago Kamta, G., and Bandrauk, A. D. (2005). *Phys. Rev. A* **71**, 053407.
[70] Gordon, A., and Kärtner, F. X. (2005). *Phys. Rev. Lett.* **95**, 223901.
[71] Kjeldsen, T. K., and Madsen, L. B. (2006). *Phys. Rev. A* **73**, 047401(Comment).
[72] Usachenko, V. I. (2006). *Phys. Rev. A* **73**, 047402(Reply).
[73] Zimmermann, B., Lein, M., and Rost, J. M. (2005). *Phys. Rev. A* **71**, 033401.
[74] Salières, P., *et al.*, private communication.
[75] Vozzi, C., *et al.* (2005). *Phys. Rev. Lett.* **95**, 153902.
[76] Wabnitz, H., *et al.* (2006). *Eur. Phys. J. D* **40**, 305.
[77] Kanai, T., Takahashi, E. J., Nabekawa, Y., and Midorikawa, K. (2007). *Phys. Rev. Lett.* **98**, 153904.
[78] Patchkovskii, S., Zhao, Z., Brabec, T., and Villeneuve, D. M. (2006). *Phys. Rev. Lett.* **97**, 123003.
[79] Patchkovskii, S., Zhao, Z., Brabec, T., and Villeneuve, D. M. (2007). *J. Chem. Phys.* **126**, 114306.
[80] Lein, M., de Nalda, R., Heesel, E., Hay, N., Springate, E., Velotta, R., Castillejo, M., Knight, P. L., and Marangos, J. P. (2005). *J. Mod. Opt.* **52**, 465.

[81] Chelkowski, S., Zuo, T., Atabek, O., and Bandrauk, A. D. (1995). *Phys. Rev. A* **52**, 2977.
[82] Kulander, K. C., Mies, F. H., Schafer, K. J. (1996). *Phys. Rev. A* **53**, 2562.
[83] Qu, W., Chen, Z., Xu, Z., and Keitel, C. H. (2001). *Phys. Rev. A* **65**, 013402.
[84] Feuerstein, B., and Thumm, U. (2003). *Phys. Rev. A* **67**, 063408.
[85] Lein, M., (2005). *Phys. Rev. Lett.* **94**, 053004.
[86] Chirilă, C. C., and Lein, M. (2006). *J. Mod. Opt.* **53**, 113.
[87] Chirilă, C. C., and Lein, M. (2006). *J. Phys. B* **39**, S437.
[88] Santra, R., and Gordon, A. (2006). *Phys. Rev. Lett.* **96**, 073906.
[89] Urbain, X., *et al.* (2004). *Phys. Rev. Lett.* **92**, 163004.
[90] Lein, M. (2007). *J. Phys. B* **40**, R135.